Simultaneous detection of added mass and change in stiffness using micromechanical resonators

---

Master Thesis

in Nanoscience, Major in Physics

University of Basel

Raphael Grüter

Supervising tutors
Prof. Hans Hug, University of Basel
Dr. Bart Hoogenboom and Dr. Rachel McKendry, University College of London

May 2009

Abstract

Micro- and nanomechanical resonators can be used as label-free sensors. Due to adsorption of an analyte the resonance frequency of the resonator is shifted. This frequency shift depends on both mass and rigidity of the adsorbed layer, complicating the interpretation of the sensor response. In this master thesis a model describing the effects of mass and mechanical properties of an adsorbed layer onto the resonance frequency of cantilevers is presented.

Due to the adsorption of an analyte as well the quality factor is changed. A model is presented to describe the dependence between mass, stiffness and quality factor. The changes in resonance frequency and quality factor after adsorption of e-beam evaporated thin gold and copper layers are measured. The mass (density) and stiffness (Young's modulus) of these metals are well-known. Therefore, the models and theoretical predictions are tested.

By simultaneous measurement of resonance frequency and quality factor response, the effects of added mass and change in rigidity are disentangled. Furthermore the homo- and heterogeneity of the adsorbed layer strongly influences the rigidity of the coating and therefore the sensor signal. Thus, resonators are used for determination of the mechanical properties (Young's modulus) or structure of thin copper and gold layers.

List of contents

1. Introduction

1.1. Cantilever based sensors

Microcantilevers were first fabricated and designed for use as force sensors in atomic force microscopes. Because of the high force sensitivity of these devices the AFM was established as a microscopy technique with extremely high resolution and as a tool for measuring forces between surfaces[1]. Furthermore, the expansion of AFM techniques has benefited from the commercialization of microfabricated cantilevers of silicon or silicon nitride. This fact and the ability to translate a microscopic effect into a macroscopic signal made the cantilever technique as well interesting for applications in biophysics or sensor technology. Thus, cantilevers can act as physical, chemical or biological sensors[2-7].

Cantilever based sensors are coated with a sensing film or receptor molecules. Target molecules are attached to this sensitized surface when the gaseous or liquid sample solution is flowed over the sensor. The cantilever works like a transducer, which produces a signal proportional to the target concentration. Like AFM cantilevers, cantilever sensors can generally be operated in either static or dynamic mode and the similar readout systems are used.

In static mode the deflection of the cantilever is monitored. This bending can be due to a number of processes such as differential surface stress caused by molecular adsorption or chemical reactions or changes in temperature. Adsorption-induced deflections are attributed to changes in the surface free energy and are observed only when a differential adsorption occurs between the cantilever surfaces[6,7]. Therefore, only one side of the cantilever is coated with sensing molecules. The cantilever deflection for given position on the cantilever and Young's modulus and thickness of the cantilever is proportional to the differential surface stress.

But the adsorption of a layer not only changes the deflection but as well the mass and stiffness of the cantilever. These changes lead to a shift in the resonance frequency of the cantilever[8]. In dynamic mode this shift is read out measuring the thermal noise spectrum of the cantilever. Cantilever resonators are commonly used as mass sensors[4]. Assuming constant spring constant the change in mass and consequently the added mass can be determined out of the shift in resonance frequency. However, this assumption is only correct for locally placed targets or for adsorbed materials with small Young's modulus, whereas for homogeneous distributed thin layers the spring constant of the cantilever is as well altered. Therefore, mass and rigidity should both be taken into account to interpret the observed frequency shifts. In this master thesis a model is presented characterizing the effects of added mass and change in stiffness onto the resonance frequency of resonators.

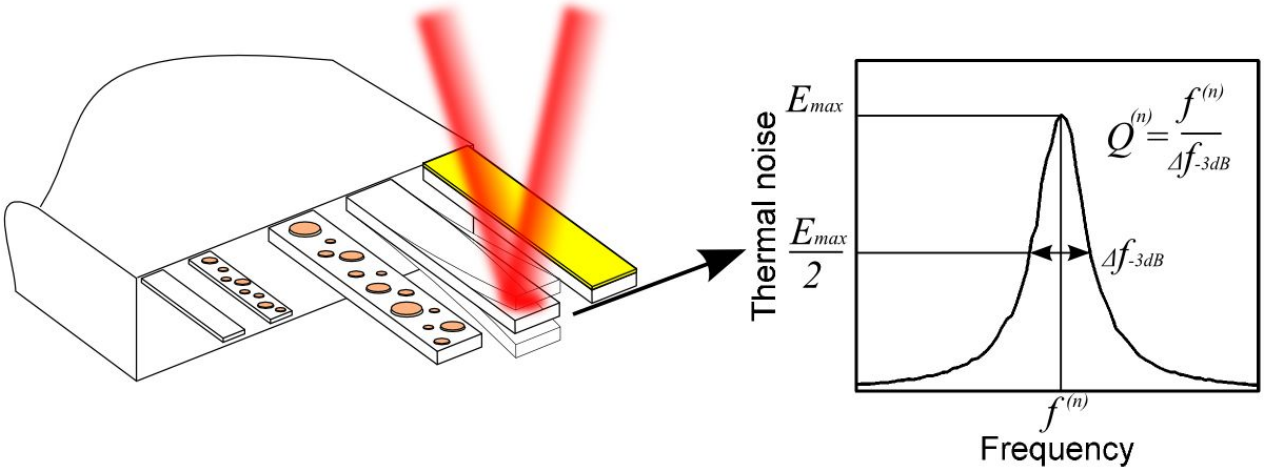

Figure 1.1: Schematics of the experimental configuration. Cantilevers covered on one side with different adsorbate layers oscillate around their equilibrium position, driven by thermal fluctuatons. Optical techniques are used to determine the thermal noise spectrum of the cantilevers, which is peaked around resonance frequencies $f^{(n)}$ with respective quality factors $Q^{(n)}$.

The rigidity of the layer strongly depends on the adsorbate homo- or heterogeneity. Therefore, a method to disentangle the effects of mass and rigidity is of main interest, in order to analyze the frequency response without a priori knowledge of the adsorbate properties. Thus, in this master thesis a second dynamical sensor property is exploited; the quality factor. The quality factor is a dimensionless parameter that compares the frequency at which a system oscillates to the rate at which it dissipates its energy. A higher quality factor indicates a lower rate of energy dissipation relative to the oscillation frequency and the oscillation dies out more slowly than for smaller quality factors. Therefore, a small quality factor indicates a strong damping effect of the oscillation of the resonator. The quality factor is related to the resonance frequency. Thus, the quality factor is defined as the ratio between resonance frequency $f^{(n)}$ and bandwidth $_{\Delta}f_{-3dB}$ (Figure 1.1). The bandwidth is defined as the range of frequencies where the Fourier transform of the signal has a power above half the maximum value, or −3 dB.

Additionally, based on two publications of Sader et al. the quality factor can be related to mass and rigidity of the cantilever. Therefore, a model is presented to disentangle the added mass and the change in rigidity due to the adsorption of a layer measuring the frequency and quality factor response. This combined measurement will have a wide field of applications in thin film or sensor technology.

2. Theory

In the following chapter, the relation between mass, stiffness, resonance frequency and quality factor of a resonator is discussed. In a first step the differential beam equation and its solution for the flexural displacement of uncoated cantilevers are presented. Afterwards, the effect of an inhomogeneous adsorbed layer onto the resonance frequency of a cantilever is derived. This equation can then be simplified for homogeneous layers. The layer is presented by its density, Young's modulus and thickness. Therefore, between the effects of mass and stiffness can be distinguished. In the last part, two equations of Sader et al.[13,14] are presented. They provide a relation between spring constant, mass and quality factor of the resonator in order to derive the theoretical quality factor response due to the adsorption of a homogeneous layer.

2.1. The beam equation

The flexural displacement u(x,t) of a single clamped rectangular cantilever with Young's modulus E_c, moment of inertia I, density ρ_c and cross sectional area A obeys the differential equation[9]:

$$\frac{\partial^2}{\partial x^2}\left(E_c I \frac{\partial^2 u(x,t)}{\partial x^2}\right) + \rho_c A \frac{\partial^2 u(x,t)}{\partial t^2} = 0 \tag{2.1}$$

The moment of inertia of a rectangular cantilever is defined by the width w and the thickness t_c of the cantilever:

$$I = \frac{w t_c^{\,3}}{12} \tag{2.2}$$

Assuming a harmonic transverse vibration, the flexural displacement u(x,t) is given by[10]:

$$u(x,t) = \sum_{i=1}^{\infty} A_i \psi_i(x) \sin(\omega_i t + \delta_i) \tag{2.3}$$

where Ψ_i is the i-th eigenmode shape, ω_i is the i-th angular eigenfrequency of the cantilever, A_i the amplitude and δ_i the phase for mode i.

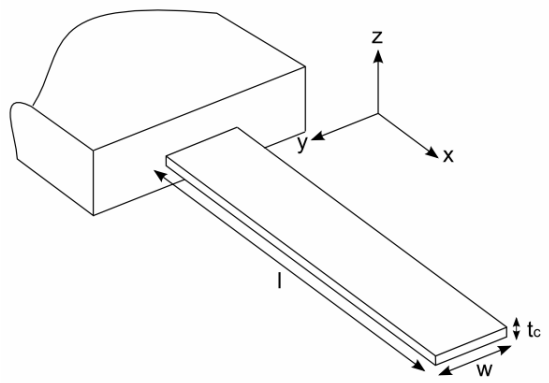

Figure 2.1: Schematic illustration of a rectangular cantilever with dimensions and coordinate system. The origin of the coordinate system is at the centre of mass of the beam cross section at its clamped end.

The eigenmode shapes of the unloaded cantilever are given by:

$$\psi_i(x) = (\sin\alpha_i + \sinh\alpha_i)\left(\cos\left(\frac{\alpha_i}{l}x\right) - \cosh\left(\frac{\alpha_i}{l}x\right)\right) - (\cos\alpha_i + \cosh\alpha_i)\left(\sin\left(\frac{\alpha_i}{l}x\right) - \sinh\left(\frac{\alpha_i}{l}x\right)\right)$$

(2.4)

where l is the length of the cantilever and the eigenvalues α_i are given by[11]:

$$\alpha_i = 1.8751,\quad 4.6941,\quad 7.8548,\quad 11.9955,\quad 14.1372.....$$

(2.5)

2.2. Coated cantilever

Assuming an adsorbed layer distributed homogeneously over the width of the cantilever with a position dependent thickness of $t_a(x)$, density ρ_a and Young's modulus E_a the Young's modulus of the cantilever is given by[12]:

$$E_{eff}(x) = \frac{E_a^2\left(\frac{t_a(x)}{t(x)}\right)^4 + E_c^2\left(\frac{t_c}{t(x)}\right)^4 + 2E_aE_c\frac{t_a(x)t_c}{t(x)^2}\left(2\left(\frac{t_a(x)}{t(x)}\right)^2 + 2\left(\frac{t_c}{t(x)}\right)^2 + 3\frac{t_a(x)t_c}{t(x)^2}\right)}{E_a\frac{t_a(x)}{t(x)} + E_c\frac{t_c}{t(x)}}$$

(2.6)

where $t(x)=t_c+t_a(x)$ is the total thickness of cantilever plus adsorbed layer. Through formation of the fractions:

$$E = \frac{E_a}{E_c},\quad T(x) = \frac{t_a(x)}{t_c}$$

(2.7)

the effective Young's modulus can be written as:

$$E_{eff}(x) = \frac{E_c t_c^3}{t(x)^3}\frac{1}{1+ET(x)}\left\{1 + E^2T(x)^4 + 2ET(x)\left[2T(x)^2 + 2 + 3T(x)\right]\right\} = \frac{12D(x)}{wt(x)^3}$$

(2.8)

The flexural rigidity D(x) is defined by[8]:

$$D(x) = \frac{D_0}{1+ET(x)}\left\{1 + E^2T(x)^4 + 2ET(x)\left[2 + 3T(x) + 2T(x)^2\right]\right\}$$

(2.9)

where D_0 is the flexural rigidity of the unloaded cantilever:

$$D_0 = \frac{E_c w t_c^3}{12} \tag{2.10}$$

Therefore, the beam equation for a coated cantilever can be written as:

$$\frac{\partial^2}{\partial x^2}\left(D(x)\frac{\partial^2 u(x,t)}{\partial x^2}\right) + \left(\rho_c t_c + \rho_a t_a(x)\right) w \frac{\partial^2 u(x,t)}{\partial t^2} = 0 \tag{2.11}$$

The vibration energy W of a cantilever is given by[10]:

$$W = \frac{1}{2}\int_0^l D(x)\left(\frac{\partial^2 u(x,t)}{\partial x^2}\right)^2 dx + \frac{w}{2}\int_0^l \left(\rho_c t_c + \rho_a t_a(x)\right)\left(\frac{\partial u(x,t)}{\partial t}\right)^2 dx \tag{2.12}$$

The first term accounts for potential energy, whereas the second term stands for the kinetic energy of the cantilever. For the derivative of the flexural displacement (equation 2.3) we get:

$$\left(\frac{\partial^2 u(x,t)}{\partial x^2}\right)^2 = A_n^2 \phi_n^2(x)\sin^2\left(\omega_n t + \delta\right) \quad \textit{and} \quad \left(\frac{\partial u(x,t)}{\partial t}\right)^2 = A_n^2 \psi_n^2(x)\omega_n^2 \cos^2\left(\omega_n t + \delta\right) \tag{2.13}$$

The second derivative of $\Psi_n(x)$ is replaced by:

$$\phi_n(x) = \frac{\partial^2 \psi_n(x)}{\partial x^2} \tag{2.14}$$

By integration over an oscillation cycle, the terms in equation 2.13 result in:

$$\int_0^T A_n^2 \phi_n^2(x)\sin^2\left(\omega_n t + \delta\right) = A_n^2 \phi_n^2(x)\pi \quad \textit{and} \quad \int_0^T A_n^2 \psi_n^2(x)\omega_n^2 \cos^2\left(\omega_n t + \delta\right) = A_n^2 \psi_n^2(x)\omega_n \pi \tag{2.15}$$

Therefore, the mean values of the potential and the kinetic energy per oscillation cycle for the nth vibration mode are given by:

$$\langle W_P \rangle = \frac{A_n^2}{4}\int_0^l D(x)\phi_n^2(x)dx \qquad and \qquad \langle W_K \rangle = \frac{wA_n^2}{4}\omega_n^2\int_0^l \left(\rho_c t_c + \rho_a t_a(x)\right)\psi_n^2(x)dx \tag{2.16}$$

By equalling potential and kinetic energy terms, the angular resonance frequency is calculated as:

$$\omega_n{}^2 = \frac{l\int_0^l D(x)\phi_n{}^2(x)dx}{m_c\int_0^l (1+\rho T(x))\psi_n{}^2(x)dx} \tag{2.17}$$

2.3. Homogeneous coated cantilever

Because of constant thickness of the adsorbed layer over the length of the cantilever, the thickness ratio can be simplified:

$$T = \frac{t_a}{t_c} \tag{2.18}$$

Similarly, the flexural rigidity gets independent of the x-coordinate:

$$D = \frac{D_0}{1+ET}\left\{1+E^2T^4+2ET\left[2+3T+2T^2\right]\right\} \tag{2.19}$$

Insertion of these terms into equation 2.17 results in:

$$\omega_n{}^2 = \frac{lD\int_0^l \phi_n{}^2(x)dx}{m_c(1+\rho T)\int_0^l \psi_n{}^2(x)dx} \tag{2.20}$$

Therefore, the effect of a homogeneous adsorbed layer on the resonance frequency f=ω/2π of the cantilever can be describes as:

$$\frac{f_n - f_{0n}}{f_{0n}} = \sqrt{\frac{D}{D_0(1+\rho T)}} - 1 \tag{2.21}$$

This simple equation combines the effects of added mass and stiffness due to the adsorption of a homogeneous layer. Whereas the added mass decreases the resonance frequency of the resonator, the increased stiffness simultaneously leads to an increase in the resonance frequency. Because normally both effects add to the frequency shift, they can be combined using equation 2.21. For a homogeneous thin gold layer the mass effect (E_{Au}=0GPa, ρ_{Au}=19320kg/m^3), the stiffness effect (E_{Au}=78GPa, ρ_{Au}=0kg/m^3) and the simultaneous effect of mass and stiffness (E_{Au}=78GPa, ρ_{Au}=19320kg/m^3) can be calculated for array cantilevers with t_c=940nm dependent on the thickness of the gold layer using equations 2.19 and 2.21 (Figure 2.2). This theoretical expectation will be verified later in chapter “Experiments and discussion”.

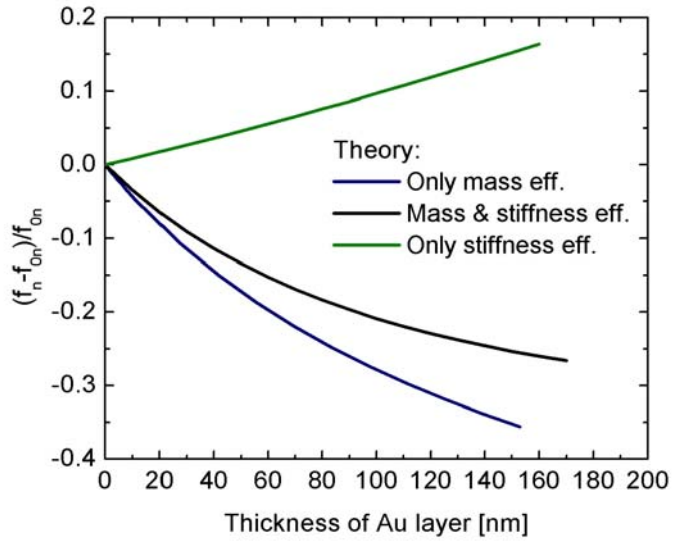

Figure 2.2: Theoretical frequency response due to adsorption of thin gold layer for array cantilever with t_c=940nm using equations 2.19 and 2.21. Mass effect only (blue) for D/D_0=1, stiffness effect only (green) for m_a=0 and simultaneous effect of change in mass and stiffness (black line).

Additionally the change in the flexural rigidity D/D_0 and the change in mass ρT are related to the ratio between added and sensor thickness T. Therefore, the thickness of the cantilever is crucial for the sensitivity of the sensor. But with decreasing thickness not only the sensitivity is increased but as well the resonance frequency of the bare sensor. Because the frequency shift is relative to this resonance frequency, the absolute frequency shift can be increased for thinner resonators.

The flexural rigidity is related with the spring constant of the cantilever by:

$$K = \frac{3D}{l^3} \tag{2.22}$$

Finally, the change in resonance frequency due to a change in spring constant and mass can be expresses as:

$$\frac{f_n - f_{0n}}{f_{0n}} = \sqrt{\frac{K}{K_0(1+\frac{m_a}{m_c})}} - 1 \tag{2.23}$$

where K_0 and K are the spring constant of the unloaded, respectively the loaded cantilever. m_a is the mass of the adsorbed layer and m_c the mass of the unloaded sensor.

The same relation is obtained for the simplified equation for the angular resonance frequency in dependence of the spring constant and the mass of the cantilever[4]:

$$\omega_{0n} = \frac{\alpha_n^2}{2\pi}\sqrt{\frac{K}{3m}} \tag{2.24}$$

This equation is used for micromechanical mass sensors. Assuming constant spring constant, the change in mass can be determined out of the change in resonance frequency.

2.4. Quality factor

Sader et al.[13] related directly the spring constant K to the plan view dimensions of the cantilever, the fundamental mode resonance frequency ω_1 , and the quality factor Q in fluid (typically in air):

$$K = 0.1906\rho_f w^2 l Q_1 \omega_1^2 \Gamma_i(\omega_1) \tag{2.25}$$

Γ_i is the imaginary component of the hydrodynamic function Γ. This equation is valid for quality factors much bigger than 1, which is typically satisfied when the cantilevers are placed in air. Additionally, knowledge of the thickness of the resonator is not required. Thus, the change in spring constant due to the adsorption of a homogeneous layer results in:

$$\frac{K}{K_0} = \frac{Q}{Q_0}\frac{\omega_1^2}{\omega_{01}^2}\frac{\Gamma_i(\omega_1)}{\Gamma_i(\omega_{01})} \tag{2.26}$$

In order to analyse the results for higher mode thermal noise measurements, a second expression can be used. Sader et al.[14] as well presented an equation for the quality factor of mode n for small dissipative effects:

$$Q_n = \frac{\frac{4\mu}{\pi\rho_f w^2}\Gamma_r(\omega_n)}{\Gamma_i(\omega_n)} \tag{2.27}$$

Γ_i and Γ_r are the imaginary and the real component of the hydrodynamic function Γ. μ is the mass per unit length of the cantilever, ρ_f is density of the fluid and w is the width of the cantilever. For small dissipative effects, the effect of the medium onto the resonance frequency of mode n is given by:

$$\frac{\omega_n}{\omega_{vac,n}} = (1 + \frac{\pi\rho_f w^2}{4\mu}\Gamma_r(\omega_n))^{-1/2} \tag{2.28}$$

By insertion of equation 2.28 into equation 2.27, the quality factor of mode n results in:

$$Q_n = \frac{\frac{4\mu}{\pi\rho_f w^2}\left(\frac{\omega_n}{\omega_{vac,n}}\right)^{-2}}{\Gamma_i(\omega_n)} \tag{2.29}$$

By assumption that the effect of the medium on f_n/f_{0n} is negligible, like it is the case for the measurements in air, the effect of the adsorption of a homogeneous layer onto the quality factor of mode n can be expressed as:

$$\frac{Q_n}{Q_{0n}} = \frac{\mu}{\mu_0}\frac{\Gamma_i(\omega_{0n})}{\Gamma_i(\omega_n)} = (\rho T + 1)\frac{\Gamma_i(\omega_{0n})}{\Gamma_i(\omega_n)} \tag{2.30}$$

The ratio between the imaginary components of the hydrodynamic function of the uncoated and the coated cantilever is mode dependent. Therefore, the change in quality factor is mode dependent as well. However, the difference between different modes is rather small.

Furthermore, added mass and change in rigidity both lead to an increase in quality factor. The effect of the stiffness onto the quality factor of the resonator is small, since the stiffness only affects the frequency term in equation 2.30. For a thin gold layer the mass effect (E_{Au}=0GPa, ρ_{Au}=19320kg/m^3), the stiffness effect (E_{Au}=78GPa, ρ_{Au}=0kg/m^3) and the simultaneous effect of mass and stiffness (E_{Au}=78GPa, ρ_{Au}=19320kg/m^3) can be calculated for array cantilevers with t_c=940nm dependent on the thickness of the gold layer using equations 2.19, 2.21 and 2.30 (Figure 2.3). This theoretical expectation will be verified later in chapter “Experiments and discussion”.

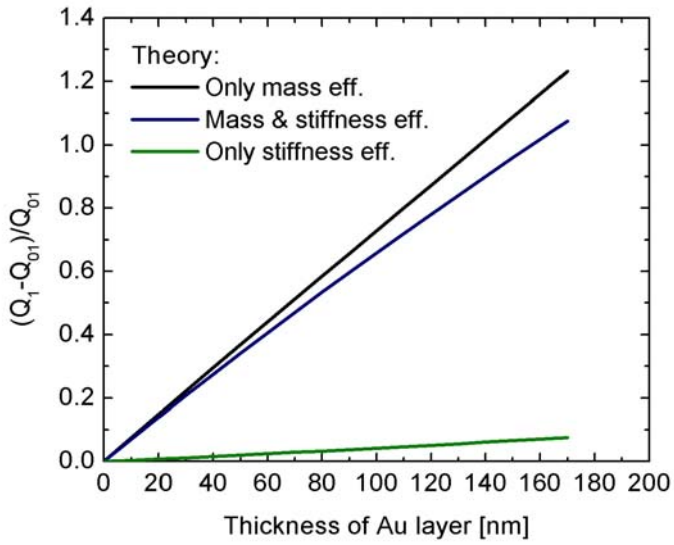

Figure 2.3: Theoretical quality factor response due to adsorption of thin gold layer for array cantilever with t_c=940nm using equations 2.19, 2.24 and 2.30. Mass effect only (blue) for D/D_0=1, stiffness effect only (green) for m_a=0 and simultaneous effect of change in mass and stiffness (black line).

2.5. Summary

In order to summarize the theoretical model, the three main equations can be extracted. The frequency response of a resonator due to the adsorption of a layer is related to the changes in mass and rigidity by equation 2.21:

$$\frac{f_n - f_{0n}}{f_{0n}} = \sqrt{\frac{D}{D_0(1+\rho T)}} - 1$$

where ρ and T are the ratios between density respectively thickness of the adsorbed layer and the cantilever. The rigidity is defined as (equation 2.19):

$$D = \frac{D_0}{1+ET}\left\{1 + E^2T^4 + 2ET\left[2 + 3T + 2T^2\right]\right\}$$

where D_0 is the flexural rigidity of the unloaded cantilever and E is the ratio between the Young's modulus of the adsorbed layer and the cantilever. Therefore, the frequency response due to adsorption of a layer with known thickness, density and Young's modulus can be predicted (Figure 2.2). Furthermore, the change in quality factor is related to the changes in mass and resonance frequency by equation 2.30:

$$\frac{Q_n}{Q_{0n}} = \frac{\mu}{\mu_0}\frac{\Gamma_i(\omega_{0n})}{\Gamma_i(\omega_n)} = (\rho T + 1)\frac{\Gamma_i(\omega_{0n})}{\Gamma_i(\omega_n)}$$

Therefore, the change in quality factor can be predicted as well (Figure 2.3). By simultaneous measurement of frequency and quality factor response due to the adsorption of a layer the added mass and change in rigidity can be disentangled and extracted.

3. Experimental details

3.1. Cantilevers

All Measurements were carried out on either arrays of “large” silicon cantilevers with dimensions of 500 µm (length) × 100 µm (width) × 940 nm (thickness) or on ultrasmall silicon cantilevers of typical dimensions 20-35 µm × 4.0 µm × 280 nm[15].

In order to improve the accuracy in length, some ultrasmall cantilevers are equipped with a “backbone”[15] at the clamped end. The “backbone” is a rigid support structure, which is attached to the support chip and overlaps onto the cantilever. Backboned cantilevers of length 25 µm (25bb) and 35 µm (35bb) were used. This backbone shortens the cantilevers and therefore redefines the length. Thus, the 25bb cantilevers are shortened down to a length of 21 µm and the 35bb cantilevers to a length of 30.5 µm. Besides, as well cantilevers without backbone and a length of 35 µm (35nb) were used.

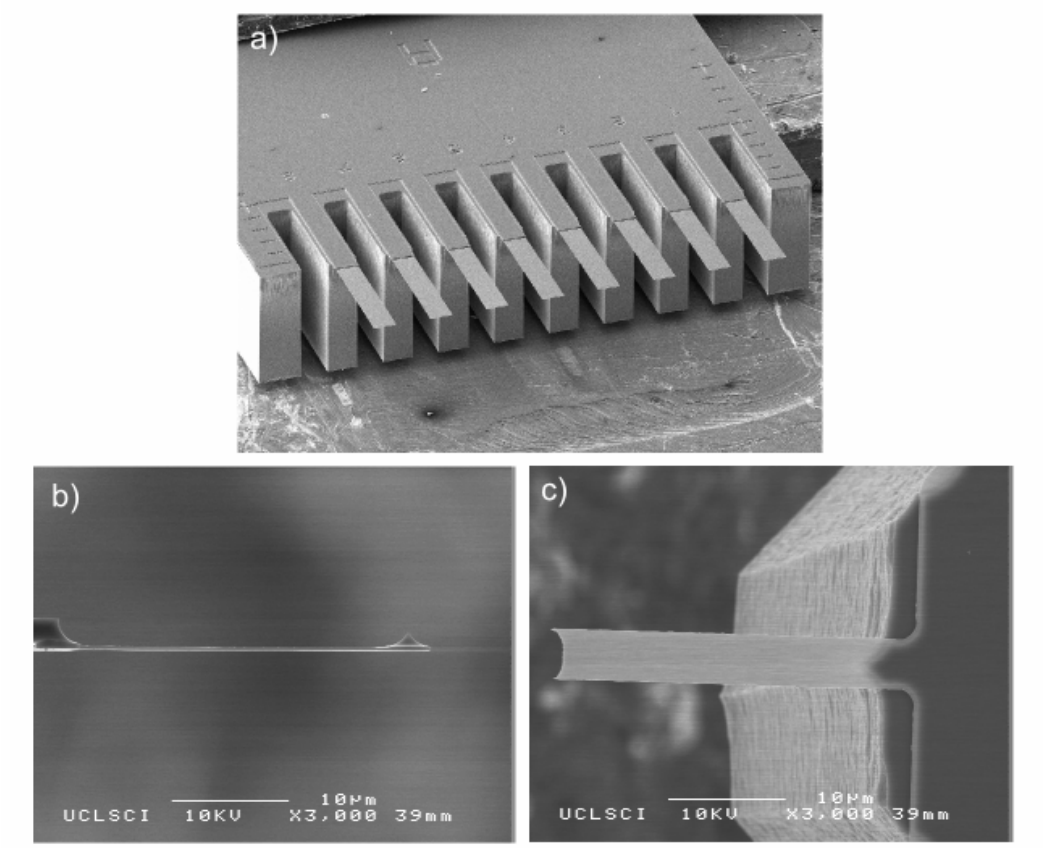

Figure 3.1: a: Top view on a cantilever array, SEM image of Ben Dueck. b: Side view of a 35bb cantilever. c: top view on a 35nb cantilever without a tip.

For all miniaturized cantilevers, the exact dimensions in length and width were determined by scanning electron microscopy (SEM) [Figure 3.1]. As it is apparent on these SEM images, some cantilevers had a defect. Because of incorrect processing, a part of the free end including the tip was missing. This error only occurred for 35nb cantilevers and shortened these cantilevers down to a length of 28 µm. However, as discussed later, the missing tip was of advantage.

3.2. Readout systems

Thermal noise spectra of the large cantilevers were measured by optical beam deflection in a commercially available atomic force microscope (JPK Nanowizard). In the optical deflection technique, the laser beam is focused and reflected on the cantilever to later impinge on a four-cell photodiode. At the undeformed position of the cantilever, the laser beam illuminates the center of the four-cell photodiode. When the cantilever is bent, the laser beam is deflected and the beam spot on the photodiode is moved out of center.

The ultrasmall cantilevers were measured using a Fabry-Perot interferometer with <3 µm spot-size[16]. In a fiber optic Fabry-Perot interferometer the interference occurs between the partially reflecting end face surface of the fiber and the cantilever surface. Therefore, for monochromatic light the intensity of the signal at the detector is dependent on the distance between the end face surface of the fiber and the cantilever surface and therefore the deflection of the cantilever.

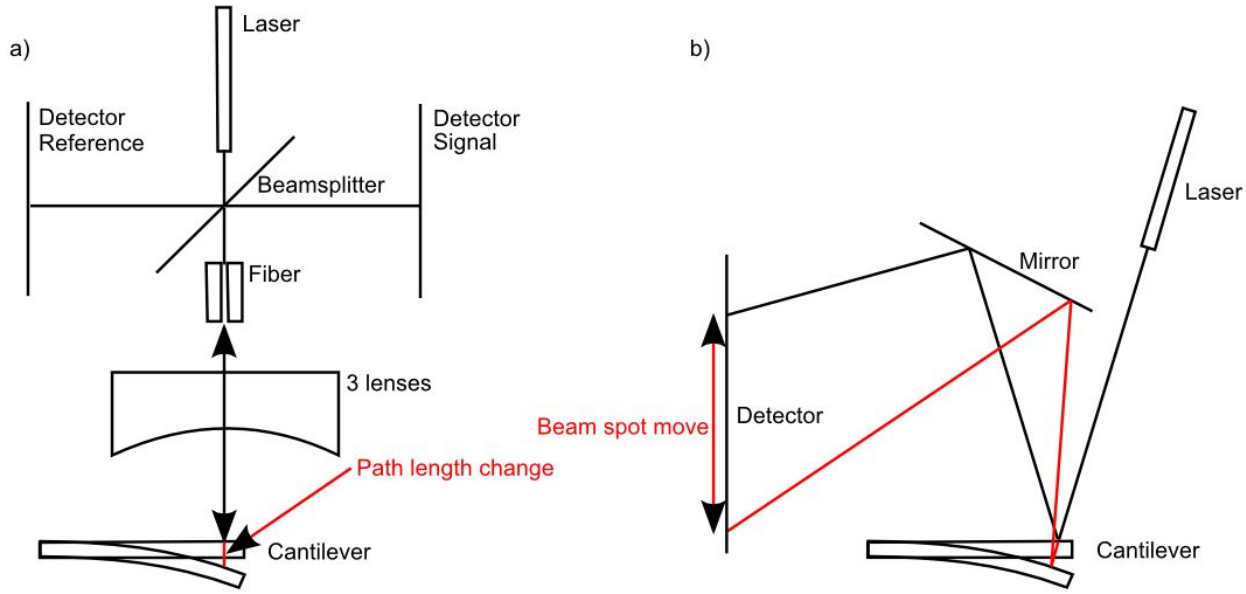

Figure 1.2: Schematic illustration of the optical laser techniques to monitor the beam deflection: Fabry-Perot interferometry (a) and optical beam deflection (b).

The thermal oscillation of a cantilever can be described as superposition of different frequencies or modes. In order to analyze the measured function of deflection versus time, the function can be Fourier transformed to get the frequency domain representation. In such a frequency spectrum of the resonator the resonance frequencies for different modes are represented by peaks. In chapter “Experiments and discussion” only the frequency spectra of the resonators are analyzed and discussed.

In all cases, the thermal noise at resonance was well above the noise floor of the optical detector and was fitted to a simple harmonic oscillator model. Measurements were recorded before and after evaporation of thin metal films and control measurement were carried out to establish that the resonance curves did not show significant alterations with time.

Main parameter specifying the sensitivity of the resonator is the thickness. Only the determination of the thickness allowed later a correct comparison between results of different cantilevers. A determination of the thickness by analyzing the SEM images was difficult and imprecise. But the thickness was determined by analysis of the measured resonance frequencies for the bare cantilevers. In Appendix C the used model-dimensions and their theoretical resonance frequencies are listed which are in good agreement with the resonance frequencies measured for uncoated cantilevers (Appendix B).

3.3. Cleaning and Evaporation

For the gold-coated cantilevers, arrays were cleaned prior to the first measurement for 20 minutes in a piranha solution, a 1:1 mixture of sulphuric acid (H_2SO_4) and hydrogen peroxide (H_2O_2). Subsequently, the substrates were rinsed three times in distilled water and once in ethanol and finally dried on a heater by 70 ºC.

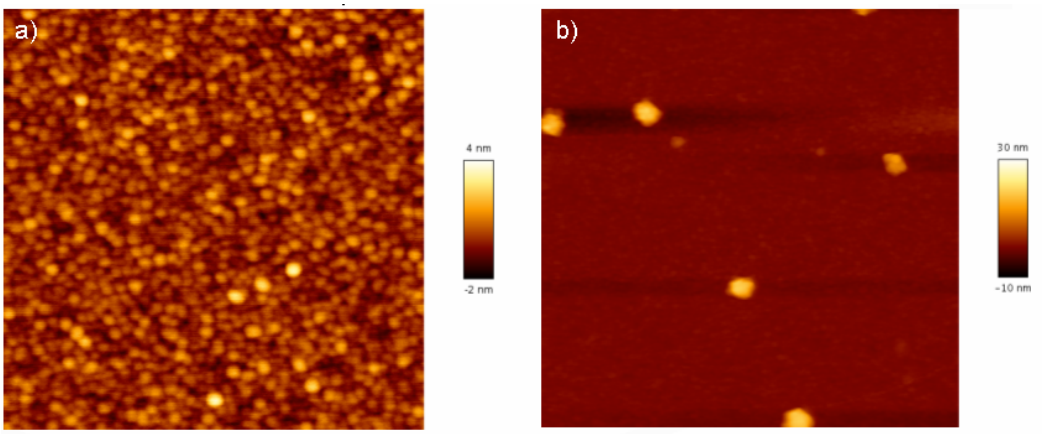

Figure 3.2: AFM images of copper on silicon wafer. Image size is 1 × 1 μm². a: 5 nm Cu with evaporation rate of 0.09 nm/sec, b: 3 nm Cu with evaporation rate of 0.01 nm/sec.

Thin metal films were evaporated on the cantilevers by e-beam evaporation in a vacuum chamber (10^{-7} mbar base pressure) at room temperature. Different thicknesses of either gold (rate: 0.09nm/sec) or copper (rate: 0.01 nm/sec) were deposited on the cantilevers. For the fixation of the gold layer, an additional 2 nm titanium adhesion layer was evaporated prior to the gold layer (rate: 0.03 nm/sec).

A low evaporation rate was chosen for copper in order to create a layer affecting only mass but not stiffness of the cantilever. For such low evaporation rates copper shows island growth[17]. Therefore, the copper islands should not interact and the copper layer should not influence the stiffness of the resonator. Prior to the experiments the copper growths was studied on silicon wafer in order to choose optimal conditions for island growth (Figure 3.2).

3.4. Data Analysis

The AFM tip of the ultrasmall cantilevers has a non-negligible effect on the resonance frequency of the cantilevers. The additional mass at the end of the cantilever influences strongly the sensitivity of the sensor and therefore decreases the frequency shift. To facilitate comparison to the theoretical model and between cantilevers of different size, the measured resonance frequencies have been corrected. For this, the tip was represented by an additional silicon layer of 300 nm thickness over the whole width of the last 3 μm of the cantilever. This equals in volume and mass the dimension of a tip, which could be described as a cone of height 1.5 μm and radius 1.5 μm and was in good agreement with the SEM measurements (figure 3.3).

In contrast to the volume, the exact shape of the tip was not critical. Thus, calculations replacing the rectangular shape with height 300 nm with an isosceles triangular shape of height 600 nm resulted in insignificant differences.

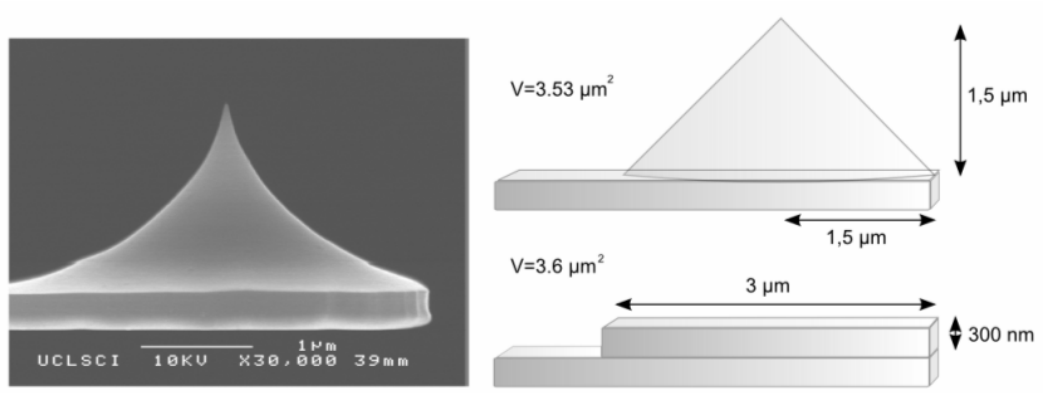

Figure 3.3: SEM image of the AFM tip and the models, representing the tip as a cone and a homogeneous layer.

Using equation 2.17 for inhomogeneous layers the theoretical frequency shift due to the adsorption of a copper layer for a cantilever with tip was calculated (figure 3.4). The effect of this additional mass at the end of the cantilever onto the frequency shift is dependent on length and shape of the cantilever. Therefore, the tip affects more the frequency shift of the shorter 25bb cantilevers than the shift of the 35bb cantilevers.

The rigidity of the adsorbed layer is dependent on the homo- and heterogeneity of the layer. For adsorbed islands the rigidity is not changed at all (E=0), whereas for a homogeneous layer the rigidity affects the sensor signal ($E=E_{Cu/Au}$). For a correct subtraction of the tip effect this has to be taken into account. For adsorption of a copper or gold layer with thickness t_a the difference between the tip-corrected frequency shift Δf_{neu} and the theoretical curve without tip and total stiffness effect ($E=E_{Cu/Au}$) is related to the difference between the measured frequency shift Δf and the theoretical curve with tip and total stiffness effect ($E=E_{Cu/Au}$) by:

$$\left(\Delta f_{neu}(t_a) - \Delta f_{notip,E=E_{Cu/Au}}(t_a)\right) = \left(\Delta f(t_a) - \Delta f_{tip,E=E_{Cu/Au}}(t_a)\right)\frac{\Delta f_{notip,\Delta E}(t_a)}{\Delta f_{tip,\Delta E}(t_a)} \tag{3.1}$$

$\Delta f_{notip,\Delta E}$ is defined as the total frequency shift due to the change in rigidity for cantilevers without tip:

$$\Delta f_{notip,\Delta E}(t_a) = \Delta f_{notip,E=0}(t_a) - \Delta f_{notip,E=E_{Cu/Au}}(t_a) \tag{3.2}$$

and $\Delta f_{tip,\Delta E}$ is defined as the total frequency shift due to the change in rigidity for cantilevers with tip:

$$\Delta f_{tip,\Delta E}(t_a) = \Delta f_{tip,E=0}(t_a) - \Delta f_{tip,E=E_{Cu/Au}}(t_a) \tag{3.3}$$

Using equation 3.1 the resulting frequency shifts for cantilevers with tip were tip-corrected to enable a comparison between cantilevers of different size (Figure 3.4). For completeness, the uncorrected data are provided in Appendix B.

The frequency response is dependent on the thickness of the cantilever. Therefore, all results are plotted against the ratios t_a/t_c or $m_a/m_c=(\rho_a t_a)/(\rho_c t_c)$ in order to allow comparison between different cantilevers and with the theoretical model. The errors in t_a/t_c and m_a/m_c arise from uncertainties in the metal layer thickness (quartz crystal microbalance) and sensor thickness (SEM and resonance frequencies).

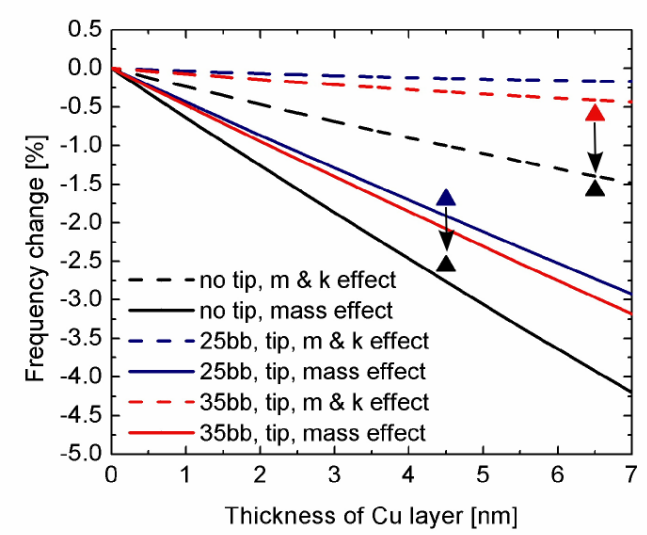

Figure 3.4: Theoretical curves for the frequency shift of resonators with (25bb: blue and 35bb: red) and without tip (black line) for effect of mass only (solid line) and simultaneous effect of added mass and change in stiffness (dashed line) in dependence of the thickness of the copper layer. Shift of the data points for cantilevers 25bb (blue) and 35bb (red) in order to correct the tip effect.

For the measurements on air, the changes in spring constant and mass were calculated inserting the measured resonance frequencies and quality factors before and after the evaporation of thin metal films into equations 2.26 respectively 2.30. Equation 2.26 was used for first mode thermal noise measurements (miniaturized cantilevers), whereas equation 2.30 was used for higher mode thermal noise measurements (cantilever arrays). In both cases the second parameter, the change in mass respectively the change in spring constant, was determined using equation 2.23.

4. Results and discussion

4.1. Model system 1: Au

4.1.1. Characterization

The cantilevers of two arrays were coated with gold layers of different thicknesses. Using glass slides as masks during two consecutive e-beam evaporations of 50 nm respectively 100 nm gold, cantilevers with gold layers of 50nm, 100nm and 150nm thickness as well as bare reference cantilevers were produced. Additionally, 20 nm gold were evaporated on three different types (35bb, 25bb and 35nb) of the miniaturized cantilevers.

For characterization, 20 nm gold were evaporated on a silicon wafer and studied under AFM. The surface of the gold layer is rough but homogeneous (Figure 4.1). In contrast to the Cu layer (chapter 4.2.) no islands are observable. Therefore, the gold layer should affect both mass and rigidity of the resonator.

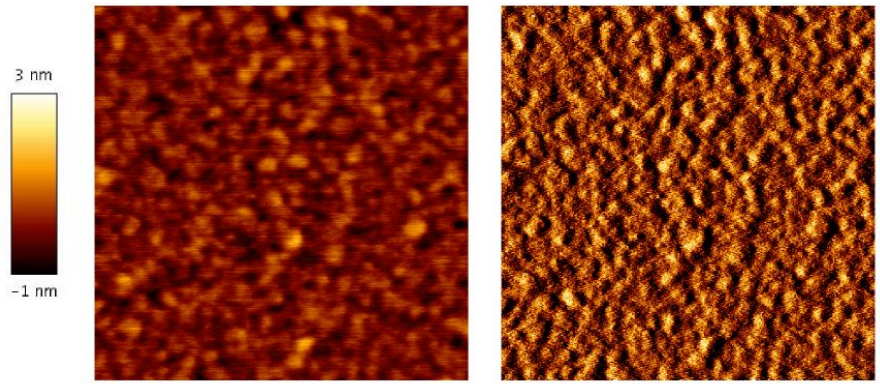

Figure 4.1: Height traces (left) and lateral deflection curves (right) for e-beam evaporation of 20 nm gold on silicon wafer with an evaporation rate of 0.09 nm/sec. The image size is 1× 1 μm².

4.1.2. Resonance frequency measurements

In air and in liquid (distilled water) the thermal noise spectrum of the array cantilevers before and after evaporation was measured. Prior to the evaporation all cantilevers of the same array had the same resonance frequencies. After the evaporation, the resonance frequencies were shifted depending on the thickness of the gold layer. For measurements in air (Figure 4.2), the resonance frequency decreased with increasing thickness of the gold layer. Additionally the amplitude was reduced for thicker gold layer what could be explained by the increase in stiffness due to the gold layer.

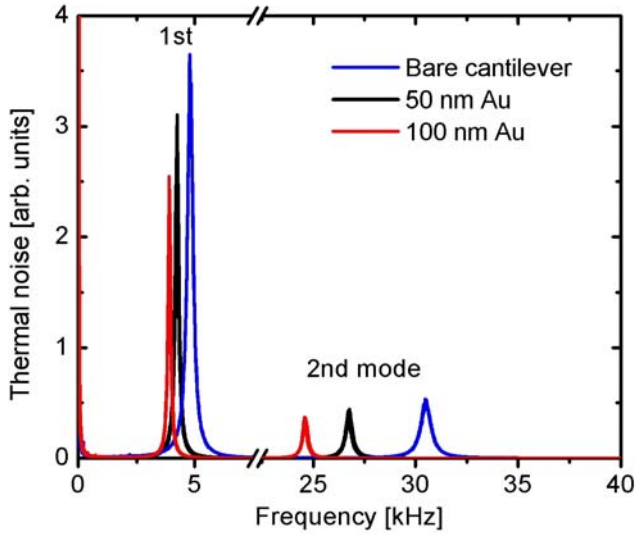

Figure 4.2: Thermal noise spectra on air with 1st and 2nd mode peaks for array cantilevers coated with gold layers of 50 and 100 nm thickness and for bare reference cantilevers (all cantilevers from same array).

As well for the measurements in distilled water a clear effect of the coating gold layer was observable (Figure 4.3). However, the direction of the frequency shift was inversed and the resonance frequencies were increased with increasing thickness of the gold layer.

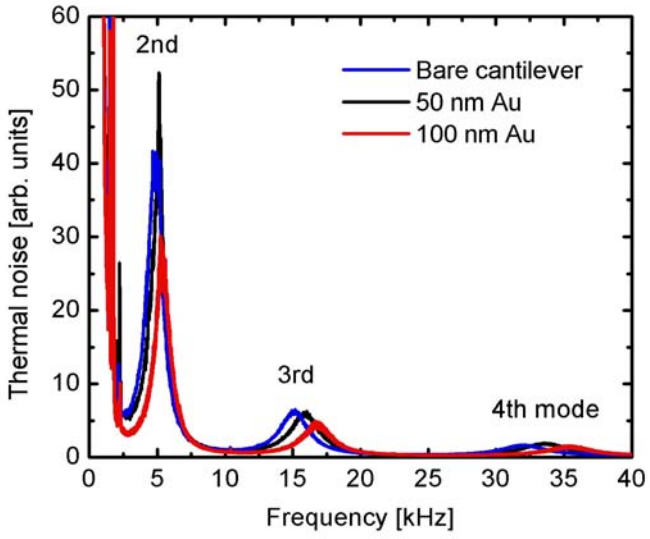

Figure 4.3: Thermal noise spectra in distilled water with 2nd, 3rd and 4th mode peaks for cantilevers coated with gold layers of 50 and 100 nm thickness and for bare reference cantilevers (all cantilevers from same array).

The relative frequency shift $(f_n-f_{0n})/f_{0n}$ due to the adsorption of gold can be compared to the theoretical calculations. In Figure 4.4 the relative frequency shifts are plotted in dependence of $m_a/m_c=(\rho_a t_a)/(\rho_c t_c)$. As calculated in equation 2.20, the shift in resonance frequency is mode independent for a homogeneous layer. The bare reference cantilevers showed no visible change in resonance frequency. Furthermore, the added mass as well as the change in stiffness added to the shift in resonance frequency for the measurements on air what validates equation 2.21.

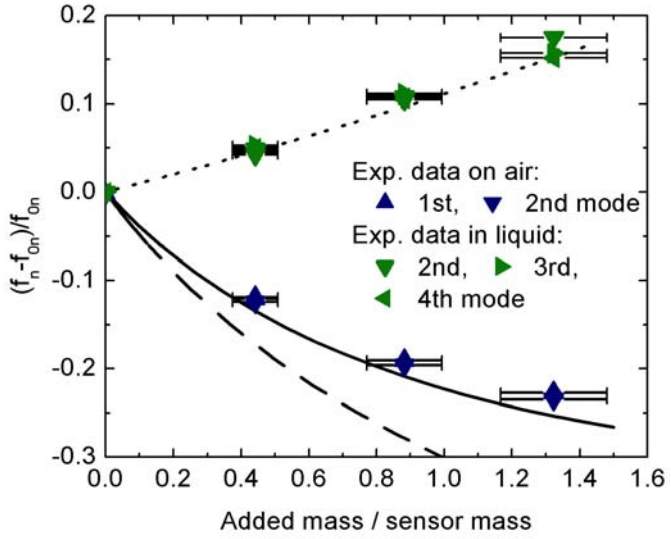

Figure 4.4: Change in resonance frequency for measurements on air (blue) and in liquid (green) in dependence of the mass of the gold layer m_a/m_c. Theoretical curves for the effects of the change in mass (dashed black line), in stiffness (dotted black line) and the simultaneous effect of mass and stiffness (black line) due to the coating gold layer.

However, in liquid only the change in stiffness seemed to add to the shift in resonance frequency. The reduced effect of the added mass can be explained by the increase in the effective sensor mass due to the water layer displaced during cantilever oscillation. Especially for lower modes this additional sensor mass seemed to reduce the ratio ρT drastically.

Additionally, the thermal noise spectrum of the miniaturized cantilevers before and after evaporation was measured in air. The sensor signal seemed to be dependent on the shape of the cantilever (Figure 4.5). For the cantilevers with tip, the frequency shift is significantly smaller than for the cantilever without tip what is in good agreement with the theoretical tip-correction (chapter “Materials and methods”). Additionally, the frequency shift for the short cantilever with tip (25bb) is smaller than for the longer cantilever with tip (35bb). Therefore, the assumption of similar shape and mass of the tips for all cantilevers seems to be correct.

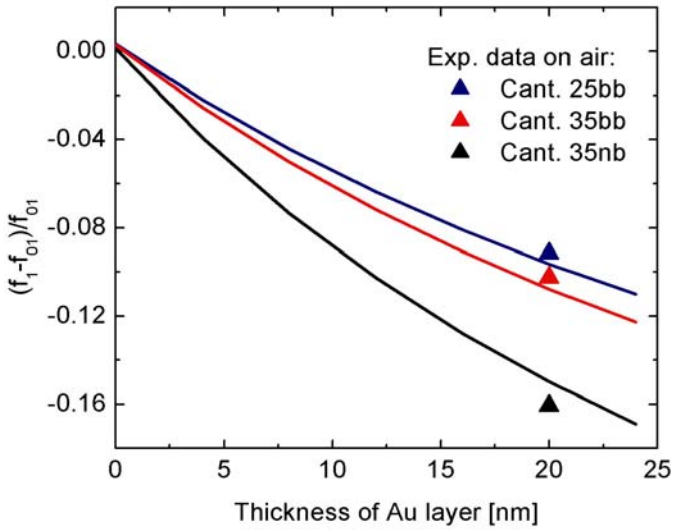

Figure 4.5: Change in resonance frequency of miniaturized cantilevers due to adsorption of 20 nm gold for measurements on air. Theoretical curves for simultaneous effects of change in mass and stiffness for 35nb cantilever without tip (black line), 35bb cantilever with tip (red line) and 25bb cantilever with tip (blue line).

After tip-correction the frequency shift for the miniaturized cantilevers are identical. Plotting the changes in resonance frequency due to the evaporation of a homogeneous gold layer in dependence of the ratio between gold layer mass and sensor mass, the results for resonators with different shapes and thicknesses can be compared (Figure 4.6). For all gold layer thicknesses the results follow the theoretical curve for a simultaneous effect of added mass and stiffness. This is in good agreement with the expectations for a homogeneous gold layer.

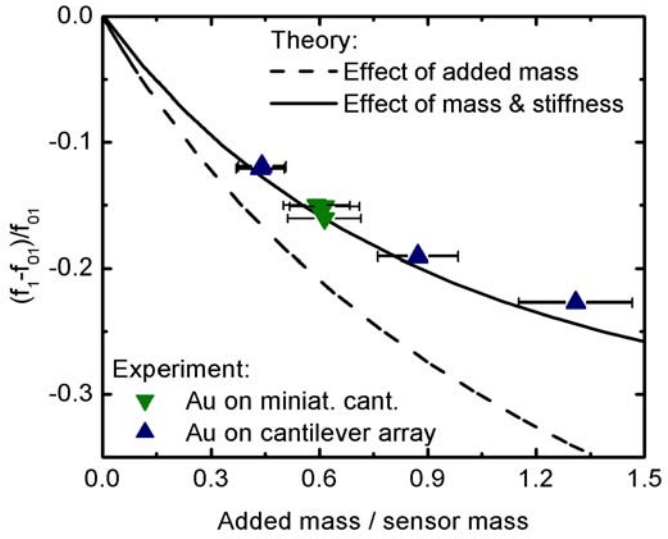

Figure 4.6: Changes in first mode resonance frequency in dependence of the ratio between the mass of the added gold layer and the sensor mass. Theoretical curves for the effects of the change in mass (dashed black line) and the simultaneous effect of added mass and stiffness (black line) due to the coating gold layer.

4.1.3. Quality factor measurement

For all resonators the quality factor increased with increasing thickness of the gold layer. This is in agreement with the theory (equation 2.30). Both, the increase in rigidity and the added mass lead to a higher quality factor. Furthermore, the quality factor shift is mode-dependent.

In figure 4.7 and 4.8 the first respectively second mode changes in quality factor are plotted in dependence of the ratio between added and sensor mass. The experimental data points clearly follow the curves taking into account the mass of the gold layer. But especially for small ratios between added and sensor mass the error in the quality factor measurement is bigger than the total stiffness effect of a homogeneous gold layer. Therefore, the results do not give evidence about the effect of the change in rigidity onto the quality factor of the resonator.

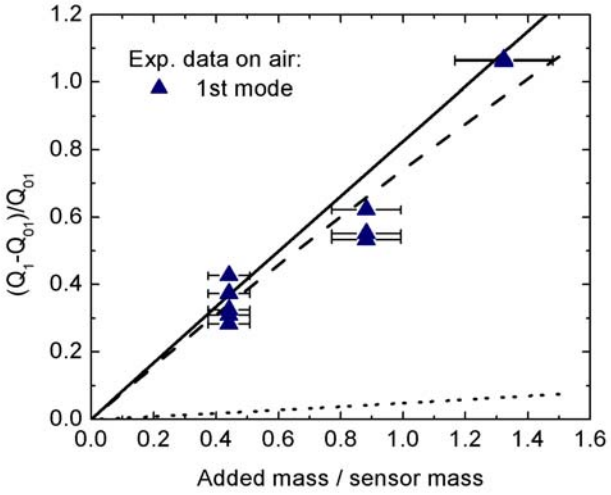

Figure 4.7: Changes in first mode quality factor in dependence of the ratio between the mass of the added gold layer and the sensor mass for array cantilever. Theoretical curves for the effects of the change in mass (dashed black line), in stiffness (dotted black line) and the simultaneous effect of mass and stiffness (black line) due to the coating gold layer.

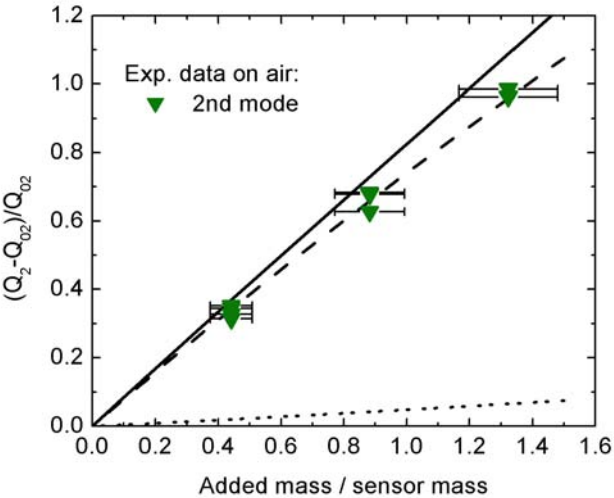

Figure 4.8: Changes in second mode quality factor in dependence of the ratio between the mass of the added gold layer and the sensor mass for array cantilever. Theoretical curves for the effects of the change in mass (dashed black line), in stiffness (dotted black line) and the simultaneous effect of mass and stiffness (black line) due to the coating gold layer.

Using equation 2.30 the added mass can be determined out of the changes in resonance frequency and quality factor. Because the mass of the adsorbed gold layer has a distinct effect onto resonance frequency and quality factor, the calculations nicely correlate with the results of the quartz crystal microbalance (figure 4.9). However, the results for second mode measurements seem to be more accurate than those for first mode.

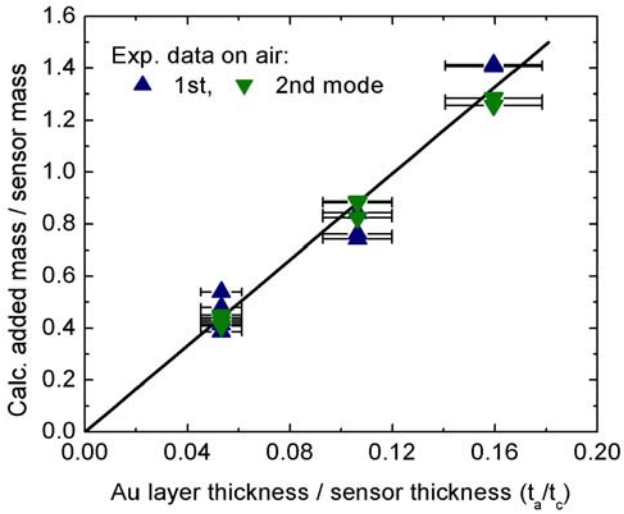

Figure 4.9: Calculated change in mass using equation 2.30 for first and second mode measurements with array cantilevers in comparison to the results of the quartz crystal microbalance (black line).

Once the added mass is determined, the change in rigidity can be calculated using equation 2.21. The effect of the change in rigidity is smaller onto both resonance frequency and quality factor of the resonator. Therefore, the error of the measurement strongly affects the accuracy of the rigidity calculations. But again the calculations for second mode measurements are more accurate than those for first mode measurements (Figure 4.10). For higher modes both resonance frequency and quality factor are higher and the absolute frequency or quality factor response is increased, what decreases the influence of the error in measurement.

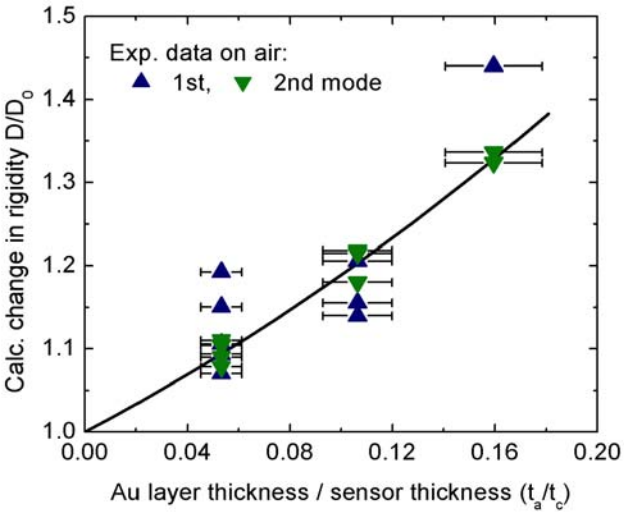

Figure 4.10: Calculated change in rigidity using equation 2.21 for first and second mode measurements with array cantilevers in comparison to the theoretical expectation for a homogeneous gold layer (black line).

With the knowledge of the plan view dimensions of the cantilever and the density of gold, the thickness of the gold layer can be determined out of the calculated change in mass (Figure 4.9). The resulting ratio $T=t_a/t_c$ and changes in rigidity D/D_0 (Figure 4.10) were inserted into equation 2.19 in order to determine the Young's modulus of the gold layer. The outcomes for second mode measurements are similar to the theoretical value of 78 GPa for all layer thicknesses (Figure 4.11). Therefore, the homogeneity of the gold coating seemed not to be dependent on the thickness of the layer. However, the results for first mode measurements show deviations to the theoretical value. As discussed earlier, the first mode measurements are affected more by the error of measurement.

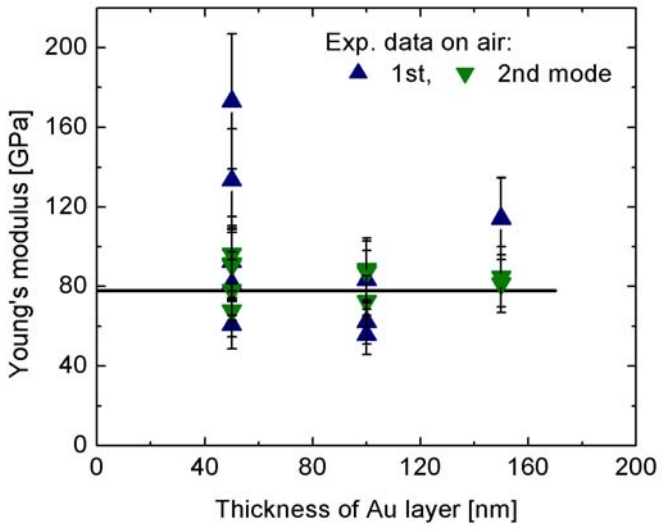

Figure 4.11: Calculated values for the Young's modulus of the gold layer in dependence of the thickness, assuming a homogeneous distribution.

4.1.4. Discussion

The experiments with homogeneous gold layers verified the effect of the change in rigidity onto the frequency response of resonators. Equation 2.21 was validated by the experiments in air. All data points matched the curve for a simultaneous effect of added mass and change in rigidity. Besides, the theoretical expectations for the change in quality factor were verified.

The relative frequency shift $(f_n-f_{0n})/f_{0n}$ is dependent on the ratios t_a/t_c or m_a/m_c. Therefore, the sensor signal is dependent on the sensor thickness. For the thinner miniaturized cantilevers the frequency response for 20 nm gold was bigger than the frequency shift for 50 nm gold on array cantilevers.

The added mass and change in rigidity can be disentangled and extracted out of the resonance and quality factor response. Furthermore as well the mechanical properties (Young's modulus) of the layer can be determined. In these experiments only first and second mode peaks were measured on air. However, the accuracy of the results would increase with higher modes due to a smaller influence of the error in measurement.

For measurements in distilled water the sensor signal was influenced by the medium. For lower modes, the water layer displaced during cantilever oscillation increased the effective sensor mass and therefore decreased the sensitivity for added mass. This problem could be reduced by reducing the plan view dimensions of the cantilever or by using higher modes.

4.2. Model system 2: Cu

4.2.1. Characterization

The rigidity of the adsorbed layer depends on its homo- and heterogeneity. Therefore, the sensor signal should be affected by the structure of the adsorbed layer. For small evaporation rates copper shows island (Vollmer-Weber) growth on native silicon oxide surfaces (chapter 3.2). Therefore, for very thin copper layers, the layer is represented by copper islands. Isolated islands do not change the rigidity of the cantilever as long as they do not touch. Thus, the coating copper film should not affect the stiffness of the resonator for very thin copper layers, whereas the elasticity of the cantilever is altered with increasing thickness of the copper layer and coalescence of the copper islands.

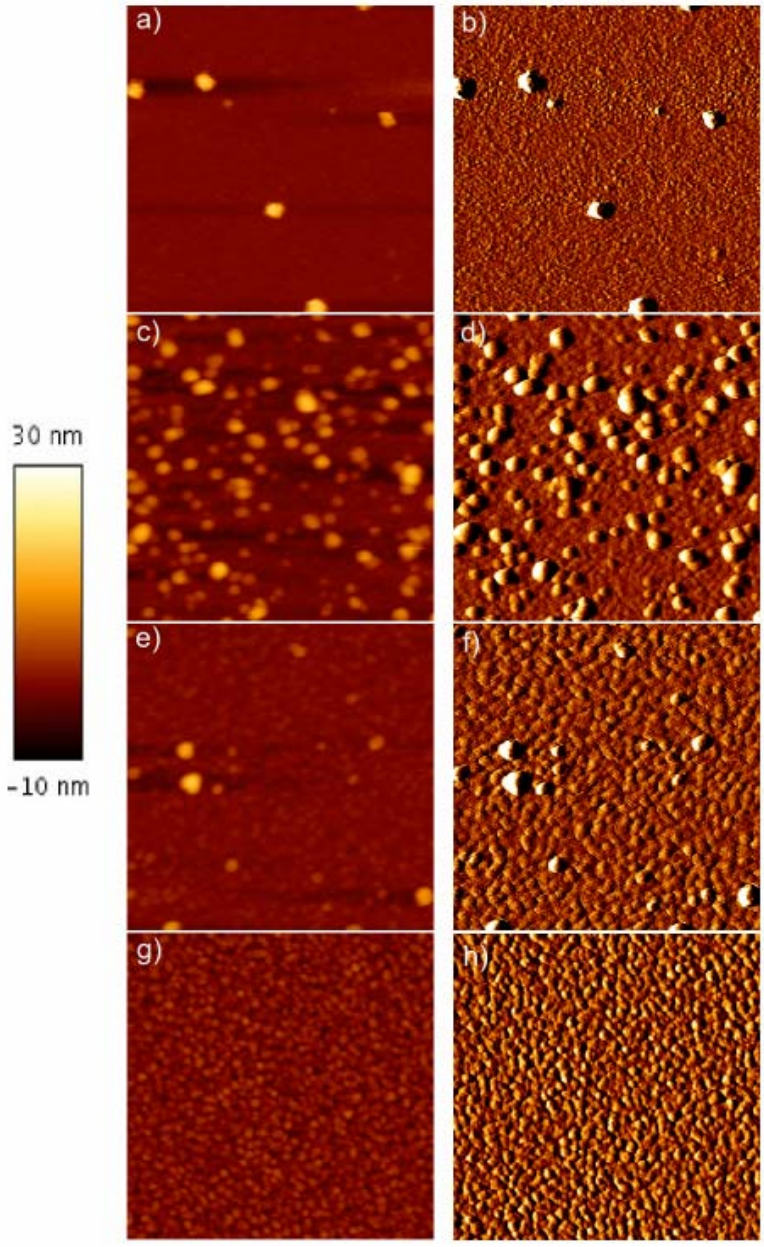

Figure 4.12: Height traces (a,c,e,g) and lateral deflection curves (b,d,f,h) for e-beam evaporation of 3 nm (a,b), 12 nm (c,d), 20 nm (e,f) and 60 nm (g,h) copper on silicon wafer with an evaporation rate of 0.01 nm/sec. The image size is 1× 1 μm^2.

Additionally, copper has a higher Young's modulus (120 GPa) than for example gold. Therefore, the rigidity effect and the dependence of the sensor signal on the homo- and heterogeneity is increased for copper layers. In order to study this effect the sensitivity of the resonators was crucial. Therefore, the miniaturized cantilevers were used for thin copper layers (3, 3.5, 12 and 20 nm), whereas a cantilever array was coated with 60 nm of copper.

The measured average layer thickness (quartz crystal microbalance) only gives information about the mass and volume but not the distribution of the copper layer. Therefore, supplementary to the cantilevers as well silicon wafers were evaporated and later studied under AFM. The height curves are shown in figure 4.12. Copper islands are present for evaporations of 3, 12 and 20 nm of copper. The number of islands increases from 3 to 12 and decreases from 12 to 20, what indicates coalescence. For 60 nm no isolated islands are visible. The surface background between the islands is getting rougher with increasing thickness of the copper layer what indicates a transition from a silicon to a copper surface.

4.2.2. Resonance frequency measurements

4.2.2.1. One evaporation

After tip-correction of the resulting frequency shifts, a clear change in the rigidity effect is observable (Figure 4.13). For average thicknesses of 3 and 3.5 nm the data points follow the theoretical curve taking into account only the change in mass. The stiffness of the cantilever seems to change for average thicknesses of 12 and 20 nm. But a homogeneous and therefore total effect of the stiffness is only observable for a copper layer of 60 nm thickness.

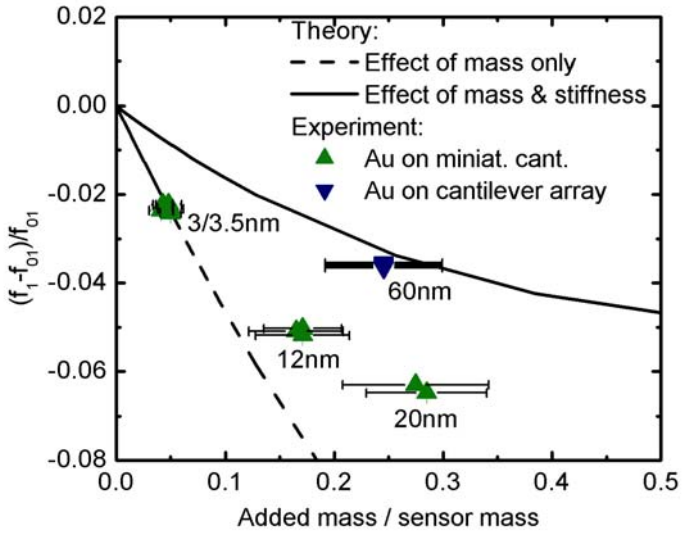

Figure 4.13: Changes in first mode resonance frequency in dependence of the ratio between the mass of the added copper layer and the sensor mass. Theoretical curves for the effects of the change in mass (dashed black line) and the simultaneous effect of added mass and stiffness (solid black line) due to the coating copper layer.

The transition of the copper layer from islands to a homogeneous layer is gradual. Therefore, during the transition, the copper layer consists of a homogeneous, affecting mass and rigidity, and a non homogeneous part, affecting only mass of the resonator. Thus, the ratio between the volume of the homogeneous part and the total copper layer (homogeneity-factor h) provides information about the stiffness effect of the layer. The theoretical frequency shift for different homogeneity-factors can be calculated using equations 2.19 and 2.20 (Figure 4.14). Interestingly, the frequency shift does not depend linearly on this ratio. Thus, for ratios smaller than 0.5 almost no stiffness effect is observable, whereas the transition from 1 to 0.9 leads to a large mass effect and frequency shift. This could explain why only the copper layer with a thickness of 60 nm showed a nearly total effect of the stiffness onto the frequency shift of the resonator.

For the experimental data points homogeneity-factors of 0 (3nm), 0.75 (12 nm), 0.85 (20nm) and 1 (60nm) can be extracted out of figure 4.14. These values will be compared to the AFM measurement in chapter “4.2.4. Discussion”.

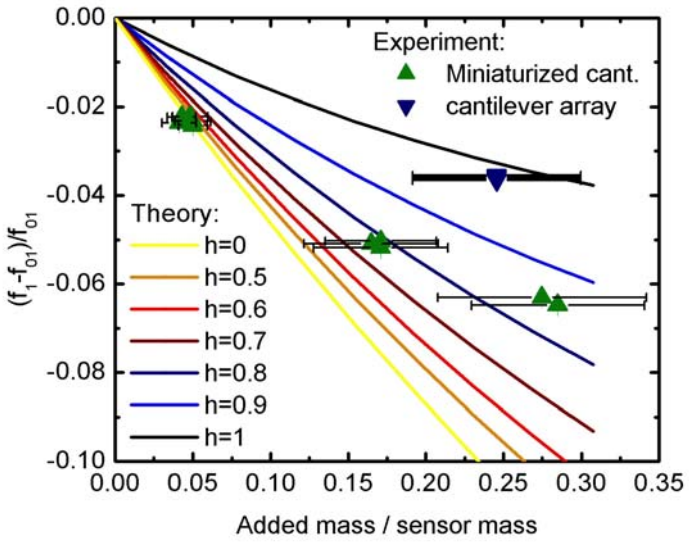

Figure 4.14: The structure of the copper layer is crucial for the size of the frequency response. The theoretical changes in resonance frequency in dependence of the ratio between added and sensor mass are calculated for different homogeneity-factors h.

Assuming a homogeneous layer distribution with known average thickness (t_a) and density, the effective Young’s modulus of the copper layer can be calculated out of the measured frequency shift using again equations 2.19 and 2.21. The results show nicely the transition between zero elasticity (no contact between islands) and total elasticity (120 GPa for bulk copper) (Figure 4.15). A negative Young’s modulus would not be possible but could be traced back to a larger frequency shift in experiment than theoretically expected.

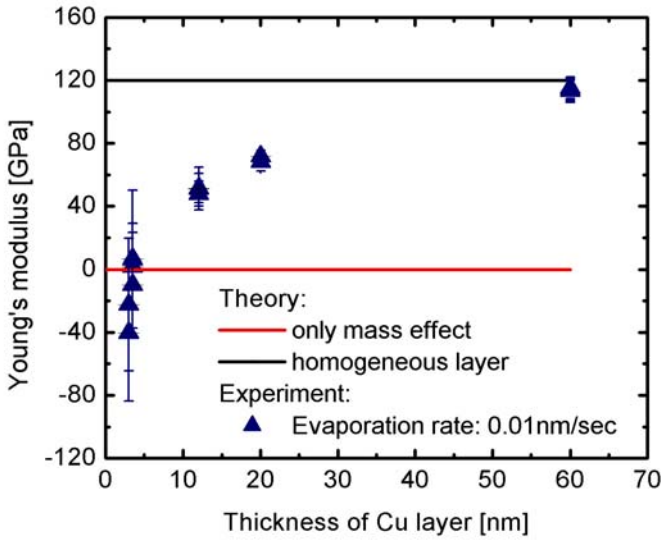

Figure 4.15: Calculated values for the Young's modulus of the copper layer in dependence of the thickness, assuming a homogeneous distribution.

4.2.2.2. Repeated evaporation

Subsequently to the first evaporation of copper, the miniaturized cantilevers were coated a second or even third time with copper. Between the evaporation cycles, the resonance frequencies of the cantilevers were measured on air. All data points for repeated evaporations showed larger frequency shifts than resulted for a single copper layer (Figure 4.16), indicating a smaller stiffness effect.

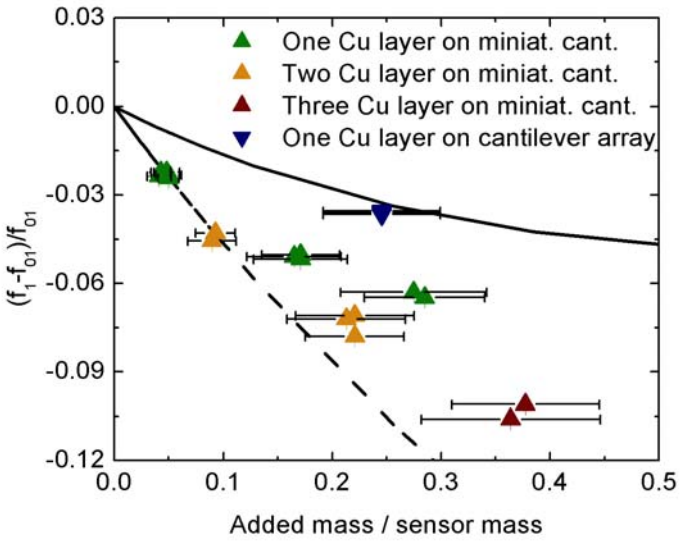

Figure 4.16: Changes in resonance frequency for copper adsorbed in one, two or three evaporation steps in dependence of the ratio between the mass of the added copper layer and the sensor mass. Theoretical curves for the effects of the change in mass (dashed black line) and the simultaneous effect of added mass and stiffness (black line) due to the coating copper layer.

An explanation could be that copper tends to oxidize on air. Therefore, the second or third copper layer was not placed onto copper but onto copper-oxide, what resulted in a copper-oxide-copper interlayer. The resonance frequency response of the resonators gives information about the mechanical properties of this copper-oxide-copper interlayer. The Young's modulus of this interlayer seems to be smaller than that one for bulk copper.

In order to understand this decreased stiffness effect of the copper-oxide-copper interlayer, the second and third copper layer can be analyzed individually (Figure 4.17). For this, the ratio between added and sensor mass is adjusted adding the existing copper layer to the sensor mass. By doing so, all data points show the same behavior. This indicates that the copper-oxide-copper interlayer has a Young's modulus of nearly zero and the new copper layer shows no interaction with the copper layer adsorbed earlier.

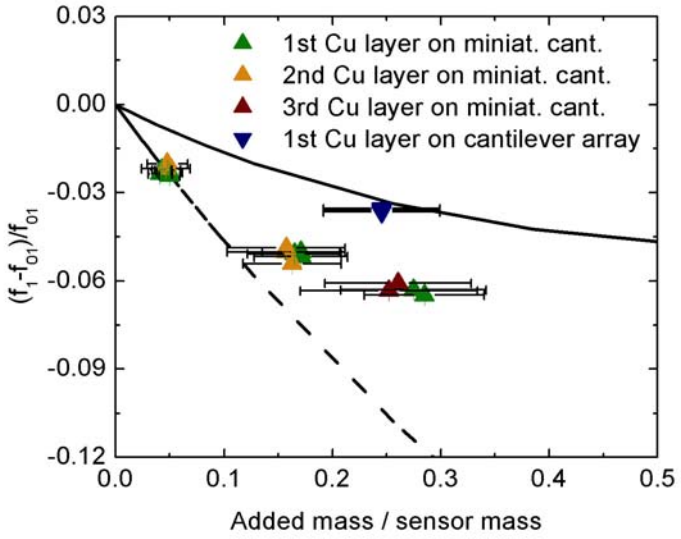

Figure 4.17: Changes in resonance frequency for copper adsorbed on bare silicon cantilevers or cantilevers coated with copper in dependence of the ratio between the mass of the added copper layer and the sensor mass. Theoretical curves for the effects of the change in mass (dashed black line) and the simultaneous effect of added mass and stiffness (black line) due to the coating copper layer.

4.2.3. Quality factor measurement

All measurements with thin copper layers were carried out using miniaturized cantilevers. Especially for the miniaturized cantilevers, the bimetallic effect[23] made an exact determination of the quality factor difficult once the cantilevers were coated with copper. This resulted in a large error in measurement. Nevertheless, the change in rigidity due to the adsorbed copper layer can be determined out of the resonance frequency and quality factor response using equation 2.26 (Figure 4.18).

The analysis of the frequency response measurements showed a gradual transition from copper islands to a copper layer with increasing thickness of the layer. The change in rigidity strongly depends on the homo- and heterogeneity of the copper layer. Therefore, the rigidity of the cantilever shouldn't be changed much for thin copper layers, what correlates with the results for 12 and 20 nm copper layers. On the other hand, the rigidity should be changed totally for a homogeneous layer (60 nm), what again correlates with the calculated change in rigidity for this layer. However, the errors in measurement are as big as the effective change in rigidity what questions the accuracy of these results.

After determination of the change in rigidity the added mass can be calculated using equation 2.21 (Figure 4.19). As well the calculated change in mass shows high variability. The errors are as large as the effective change in mass. However, the data points seem to follow the theoretical curve for a total mass effect for all copper layers. Because the mass effect is not dependent on the homo- and heterogeneity of the copper layer, this is expected.

The sensor mass is crucial for the mass sensitivity of the resonator. The mass of an array cantilever is 110 ng, whereas the miniaturized cantilevers have masses between 55-77 pg. Therefore, the miniaturized cantilevers show the same signal (frequency shift) as the array cantilevers for masses more than 3 orders of magnitude smaller.

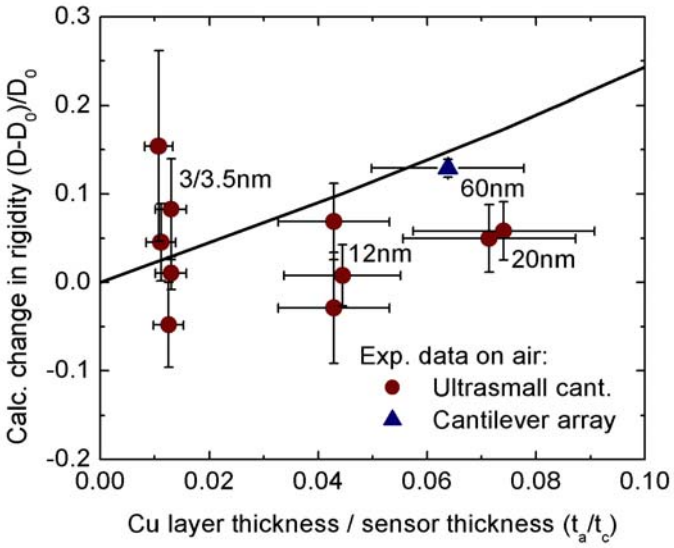

Figure 4.18: Calculated change in rigidity using equation 2.26 for first mode measurements with array cantilevers (blue) and ultrasmall cantilevers (red) in comparison to the theoretical expectations for a homogeneous copper layer (black line).

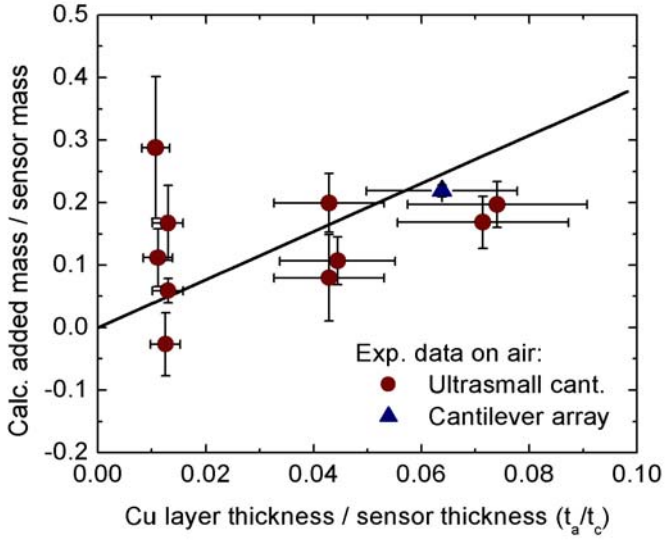

Figure 4.19: Calculated change in mass using equations 2.21 and 2.26 for first mode measurements with array cantilevers (blue) and ultrasmall cantilevers (red) in comparison to the results of the quartz crystal microbalance (black line).

4.2.4. Discussion

The results of the resonance frequency measurements correlated with the theoretical expectations. With the transition from copper islands to a homogeneous copper layer, the rigidity of the resonator started to be affected. The homogeneity-factor h was introduced to provide information about the size of the stiffness effect of the layer and was extracted out of the frequency response. However, h can be compared to the AFM measurements. Out of the histograms of the height curves the volume of the layer above a certain z-height can be extracted. Two different volumes were calculated. For $V(z\text{-}z_{min})$ the volume above the minimal z-height and $V(z\text{-}z_{peak})$ the volume above the surface peak was determined (Figure 4.1). Because the stiffness effect of the surface is dependent on the roughness and can't be evaluated accurately, the non homogeneous part of the copper layer can be located between $V(z\text{-}z_{peak})$ and $V(z\text{-}z_{min})$. Therefore, homogeneity-factors of 0.3-0.9 (3nm), 0.5-0.85 (12 nm), 0.85-1 (20nm) and 0.85-1 (60nm) are calculated.

t_a [nm]	$V(z\text{-}z_{min})$ [10^6 nm^3]	$V(z\text{-}z_{peak})$ [10^6 nm^3]
0	0.919	0.073
3	1.986	0.237
12	5.846	1.765
20	2.962	0.177
60	8.002	0.016

Table 4.1: Calculated volumes for $V(z\text{-}z_{peak})$ and $V(z\text{-}z_{min})$ for different thicknesses of adsorbed copper.

The results for average layer thicknesses >3 nm are similar to the homogeneity-factors extracted out of the frequency response. However, for a copper layer of 3 nm these results do not correlate with the frequency response measurements. An explanation could be that copper molecules tend to diffuse into the silicon surface. The rigidity of the resonator seems not to be influenced by this process.

Additionally, the effect of the oxidation of the copper layer has to be discussed. After exposure to air the copper layer will be covered by a thin oxide layer. The growth of this oxide layer is suppressed once a substantial thickness is reached. For thicker layers the effect of the additional oxide is small compared to the frequency shift due to the whole copper layer. However, the frequency shift for cantilevers coated with copper layers of 3 and 3.5 nm thickness seems to be influenced by the additional oxide layer. The mass effect and therefore the resonance shift are bigger for these films than theoretically expected. Furthermore, this could be an explanation for the negative results for Young's modulus of copper layers with average thickness of 3 and 3.5 nm.

5. Conclusion and outlook

Especially for adsorption of a layer, the frequency response of a cantilever sensor is not only dependent on mass but as well on the rigidity of the adsorbed layer. The effects of mass and stiffness onto resonance frequency can be described using equation 2.21. The measurements for adsorption of homogeneous gold layers clearly demonstrated the additional effect due to the change in stiffness. For lower mode measurements in liquid the rigidity effect even dominated the change in mass.

As shown for the measurements with copper, the frequency response as well supplies information about the homo- and heterogeneity of the layer. Additionally, information about the interaction between different layers and mechanical properties of interlayers can be extracted out of the frequency response measurements. This ability could lead to applications in thin-film technology.

By in situ measurement of both quality factor and resonance frequency, added mass and change in stiffness due to the adsorption of a layer can be directly disentangled and extracted. Therefore, it could be possible to simultaneously detect the mass of adsorbed molecules, their interaction and mechanical properties, what could be of interest in sensor technology.

However, to get accurate results, an exact definition and information about the shape of the resonators is crucial. The better it is the smaller is the error in measurement. The definition gets better for bigger cantilevers, whereas the sensitivity increases with smaller and thinner resonators. Therefore, it is important to find a middle course to improve the method. Furthermore, the shape of the cantilever could be adjusted to the sensor-target and sensor-property in order to minimize other effects.

6. Acknowledgements

Prof. Hans Hug: *For supervision of my Master Thesis at the University of Basel*

Dr. Rachel McKendry and Dr. Bart Hoogenboom: *For supervision of my Master Thesis at the University College of London*

Zermina Khan, Ben Dueck, Dr. Joseph Ndieyira, Manuel Vögtli and Marco Fritzsche: *For technical and practical support*

Swiss Nano Institute and FRONTIERS: *For financial support*

7. Appendix

A. References

[1] D. Rugar, P. K. Hansma, *Phys. Today* 43 (1990) 23
[2] G.Y. Chen, T. Thundat, E.A. Wachter, R.J. Warmack, *J. Appl. Phys.* 77, 3618 (1995)
[3] E. Finot, A. Passian and T. Thundat, *Sensors* 2008, *8*, 3497-3541
[4] T. Braun, V. Barwich, M. K. Ghatkesar, A. H. Bredekamp, C. Gerber, M. Hegner and H. P. Lang, *PHYSICAL REVIEW E* 72, 031907 (2005)
[5] J. Tamayo, A. D. L. Humphris, A. M. Malloy and M. J. Miles, *Ultramicroscopy* 86 (2001) 167-173
[6] M. L. Sushko, J. H. Harding, A. L. Shluger, R. A. McKendry and M. Watari, *Adv. Mater.* 2008, 20, 1-6
[7] M. Watari, J. Galbraith, H.-P. Lang, M. Sousa, M. Hegner, Gerber, M. A. Horton, and R. A. McKendry, *J. AM. CHEM. SOC.* 2007, 129, 601-609
[8] J. Tamayo, D. Ramos, J. Mertens and M. Calleja, *J. Appl. Phys.* 89, 224104 (2006)
[9] C. A. Van Eysden and J. E. Sader, *J. Appl. Phys.* 100, 114916 (2006)
[10] H.-J. Butt and M. Jaschke, *Nanotechnology* 6 (1995) 1-7
[11] R. Sandberg, W. Svendsen, K. Molhave and A. Boisen, *J. Micromech. Microeng.* 15 (2005) 1454-1458
[12] D. Ramos, J. Mertens, M. Calleja and J. Tamayo, *Sensors* 2007, 7, 1757-1765
[13] J. E. Sader, J. W. M. Chon and P. Mulvaney, Rev. Sci. Instrum., Vol. 70, No. 10, October 1999
[14] J. E. Sader, J. Appl. Phys., Vol. 84, No. 1, 1 July 1998
[15] J. L. Yang, M. Despont, U. Drechsler, B. W. Hoogemboom, P. L. T. M. Frederix, S. Martin, A. Engel, P. Vettiger and H. J. Hug, APPLIED PHYSICS LETTERS 86, 134101 (2005)
[16] B. W. Hoogemboom, P. L. T. M. Frederix, J. L. Yang, S. Martin, Y. Pellmont, M. Steinacher, S. Zäch, E. Langenbach, H.-J. Heimbeck, A. Engel and H. J. Hug, APPLIED PHYSICS LETTERS 86, 074101 (2005)
[17] T. Pienkosa, A. Proszynskib, D. Chocykb, L. Gladyszewskia and G. Gladyszewskib, *Microelectronic Engineering* 70 (2003) 442–446
[18] J.A. Dean, Lange's Handbook of Chemistry (15th Edition), McGraw-Hill, 1999; Section 3; Table 3.2 Physical Constants of Inorganic Compounds
[19] D.R. Lide, Chemical Rubber Company handbook of chemistry and physics, CRC Press, Boca Raton, Florida, USA, 79th edition, 1998
[20] A.M. James and M.P. Lord, Macmillan's Chemical and Physical Data, Macmillan, London, UK, 1992
[21] G.W.C. Kaye and T. H. Laby, Tables of physical and chemical constants, Longman, London, UK, 15th edition, 1993
[22] Spiering, V.L., Bouwstra, S., Spiering, R., Sensors and Actuators, A.39, 1993, 149-156
[23] http://www.nature.com/nature/journal/v432/n7020/full/nature03118.html

B. Results of resonance frequency measurements

Gold on air

				Frequency before Evaporation		Frequency after Evaporation	
Cantilever	tc [nm]	ta [nm]	ma/mc	1. mode [kHz]	2. mode [kHz]	1. mode [kHz]	2. mode [kHz]
Array	940	0	0.00	4.814	30.54	4.805	30.49
Array	940	0	0.00	4.819	30.56	4.809	30.52
Array	940	50	0.44	4.821	30.56	4.237	26.75
Array	940	50	0.44	4.812	30.53	4.232	26.72
Array	940	50	0.44	4.814	30.53	4.233	26.72
Array	940	50	0.44	4.913	31.16	4.331	27.29
Array	940	50	0.44	4.907	31.12	4.319	27.26
25bb	280	20	0.59	664.3		603.5	
35bb	270	20	0.61	316.0		283.6	
35nb without tip	270	20	0.61	455.0		381.9	
Array	940	100	0.88	4.829	30.6	3.907	24.62
Array	940	100	0.88	4.823	30.6	3.907	24.59
Array	940	100	0.88	4.822	30.58	3.901	24.57
Array	940	150	1.32	4.901	31.08	3.791	23.8
Array	940	150	1.32	4.896	31.05	3.782	23.75

Gold in liquid

				Frequency after Evaporation		
Cantilever	tc [nm]	ta [nm]	ma/mc	2. mode [kHz]	3. mode [kHz]	4. mode [kHz]
Cantilever-array	940	0	0.00	4.939	15.23	32.017
	940	50	0.44	5.155	16	33.576
	940	50	0.44	5.258	16.5	34.524
	940	50	0.44	5.274	16.48	34.611
	940	100	0.88	5.473	16.93	35.41
	940	100	0.88	5.456	16.9	35.392
	940	100	0.88	5.47	16.9	35.432
	940	150	1.32	5.928	18.18	37.962

Copper on air

				Frequency before Evaporation		Frequency after Evaporation	
Cantilever	tc [nm]	ta [nm]	ma/mc	1. mode [kHz]	2. mode [kHz]	1. mode [kHz]	2. mode [kHz]
Cantilever-array	940	0	0.00	4.807	30.46	4.804	30.44
25bb	280	3	0.04	688.6		676.3	
35bb	270	3	0.04	320.3		314.6	
25bb	280	3.5	0.05	678.1		667.6	
35bb	270	3.5	0.05	332.7		326.4	
35nb without tip	270	3.5	0.05	438.6		428.4	
25bb	280	12	0.16	651.2		631.6	
35nb with tip	280	12	0.16	294.7		281.9	
35bb	270	12	0.17	320.7		309.9	
	940	60	0.25	4.786	30.37	4.611	29.17
	940	60	0.25	4.791	30.4	4.619	29.21
	940	60	0.25	4.792	30.41	4.619	29.22
	940	60	0.25	4.798	30.43	4.628	29.26
	940	60	0.25	4.808	30.47	4.636	29.29
	940	60	0.25	4.814	30.52	4.639	29.32
25bb	280	20	0.27	656.7		637.2	
35bb	270	20	0.28	325.7		312.8	

C. Dimensions of the model and theoretical resonance frequencies

				Frequency before Evaporation	
Cantilever	l [µm]	w [µm]	tc [nm]	1. mode [kHz]	2. mode [kHz]
Cantilever-array	500	100	940	4.873	30.57
25bb	21	4	280	672	
35bb	30.5	4	270	320	
35nb without tip	28	4	270	446	
35nb with tip	35	4	280	275	

D. Results of quality factor measurements

Gold on air

				Qual. factor before Evaporation		Qual. factor after Evaporation	
Cantilever	tc [nm]	ta [nm]	ma/mc	1. mode	2. mode	1. mode	2. mode
Array	940	0	0.00	17.25	51.02	16.92	50.95
Array	940	0	0.00	16.76	49.8	16.43	50.53
Array	940	50	0.44	17.22	50.9	22.08	67.55
Array	940	50	0.44	16.9	51.26	22.12	67.31
Array	940	50	0.44	16.57	50.74	21.94	68.6
Array	940	50	0.44	16.5	52.38	22.65	70.36
Array	940	50	0.44	16.05	52.45	22.89	70.48
25bb	280	20	0.59	59.7		74.0	
35bb	270	20	0.61	32.9		50.2	
35nb without tip	270	20	0.61	30.0		45.2	
Array	940	100	0.88	18.05	51.5	27.67	83.8
Array	940	100	0.88	17.11	50.77	26.54	85.19
Array	940	100	0.88	17.08	50.04	27.7	84.21
Array	940	150	1.32	16.11	51.86	33.21	101.8
Array	940	150	1.32	16.06	51.48	33.18	102.2

Copper on air

				Qual. factor before Evaporation		Qual. factor after Evaporation	
Cantilever	tc [nm]	ta [nm]	ma/mc	1. mode	2. mode	1. mode	2. mode
Cantilever-array	940	0	0.00	16.61	51.02	16.77	50.91
25bb	280	3	0.04	49.4		58.3	
35bb	270	3	0.04	31.8		35.8	
25bb	280	3.5	0.05	56.1		54.5	
35bb	270	3.5	0.05	32.8		36.4	
35nb without tip	270	3.5	0.05	30.9		32.3	
25bb	280	12	0.16	57.4		63.9	
35nb with tip	280	12	0.16	32.0		32.9	
35bb	270	12	0.17	34.7		36.6	
	940	60	0.25	16.27	50.94	20.08	60.18
	940	60	0.25	16.38	50.68	19.69	60.24
	940	60	0.25	16.41	51.13	19.76	60.99
	940	60	0.25	16.68	51.69	19.83	60.11
	940	60	0.25	16.4	50.88	19.79	60.4
	940	60	0.25	16.69	51.39	19.91	60.38
25bb	280	20	0.27	60.8		66.5	
35bb	270	20	0.28	35.3		39.3	

E. Young's modules[19-22] and densities[18] used for theoretical calculations

Si	E [Gpa]	150
	ρ [kg/m^3]	2330
Au	E [Gpa]	78
	ρ [kg/m^3]	19320
Ti	E [Gpa]	116
	ρ [kg/m^3]	4506
Cu	E [Gpa]	120
	ρ [kg/m^3]	8960